Astronomy & Astrophysics manuscript no. output
October 13, 2025

TRINITY – first science

[1]

2025

ABSTRACT

1. Introduction

(see also Draine 2011; Martínez-González et al. 2014; Rahner et al. 2017):

Draine (2011, hereafter Dr11) Martínez-González et al. (2014, hereafter MG14) Rahner et al. (2017, hereafter Ra17)

1.1. SF, why important, what is it

The evolution of molecular clouds is controlled by a complex interplay of large-scale phenomena and microphysics: chemistry and interaction of the matter with the surrounding far-UV and cosmic-ray radiation control the thermodynamic state of the gas and its coupling to the magnetic field

To understand we need to understand stellar feedback.

We build our model on the basis of warpfield.

This problem is complex and has to be self consistent, so a large parameter space is required. With 1D, this can be achieved at low computing time.

This is a very useful simplification.

Stellar feedback is crucial in regulating star formation. It

One of the most obvious form is the formation of bubbles. Bubbles such as HII regions, wind-blown bubbles, and superbubbles. In galactic and nearby context, they are separable. In nearby galaxies, they are almost indistinguishable.

These are forged via a combination of processes, such as stellar winds, photoionisation, radiation pressure, and supernovae.

1.2. observational studies, increasing need for models

Observationally, the shells and cavities in the ISM by JWST.

1.3. current challenge, why is 1D required

While three-dimensional simulations are undoubtedly more geometrically realistic, particularly for capturing the complex, turbulent structure of the interstellar medium, they also come with substantial trade-offs. Chief among these are their high computational cost and the resulting difficulty in exploring parameter space or isolating the effects of individual physical processes. By contrast, one-dimensional, semi-analytic models like the one we present here offer a more controlled environment in which to study the fundamental physics of stellar feedback. They allow us to track key quantities — energy, momentum, mass flux — with high fidelity and at negligible computational cost, and to do so in a fully self-consistent framework without the need for sub-grid approximations. Moreover, many feedback scenarios, such as wind-driven bubbles or supernova remnants in uniform media, are well approximated by spherical symmetry, making 1D not just a toy model, but a useful first-order description. As such, our model should be viewed as complementary to more complex simulations: it does not replace them, but it provides a clean baseline against which to interpret their results and to identify which physical effects truly matter.

1.4. missing in current models, what does TRINITY address. what in observation can TRINITY clarify

NGC 628 papers, watkin bubbles. (Lee et al. 2022; Watkins et al. 2023; Pathak et al. 2025)

It would be great to be able to study relationship between radius and age of systems.

1.5. scope of paper, outline.

We consider clouds in various enrivonemnts (pressure), different initial cloud mass and cloud density, cloud profiles.

2. Science

- Dataset of the evolution of HII regions in a homogeneous cloud.
- Looking for simple relation, such as:
  - Luminosity-radius
  - age-radius
  - feedback-radius. An indirect probe of feedback strength for observations.
    - pressure component (thermal, radiation, ram) vs radius.
- Introduce small tuning of initial conditions, such as SFE and cloud mass.

3. Method

3.1. Phase 0: Initial cloud conditions

We consider a spherical cloud of mass M, and some star formation efficiency (e).

THe ISM component is standard, eg. . ie 1 helium atom per 10 hydrogen atoms, giving mean molecular weights of μ_i and μ_p of xx. The ISM density is xx, with temperature of xx.

At the early stage, the cloud in vicinity of star is blown away by stellar wind with constant terminal velocity V and

mass loss rate dM_w/dt. The mechanical luminosity L_w is therefore

$$L_w = \frac{1}{2}\frac{dM_w}{dt}V_w^2 \tag{1}$$

We describe the cloud with four main parameters, i.e., sfe, mass, metallicity, and density profile.

The initial radius of the cloud is R_{cl}, such that it satisfies the following:

$$M_{\rm cl} = 4\pi \int_0^{R_{\rm cl}} r^2 \rho(r)\,{\rm d}r \tag{2}$$

where density profiles are described in Section 5.

This free-expansion phase ends when the mass of the swept-up ISM becomes comparable to that of the ejected stellar mass (Lamers & Cassinelli 1999)

$$t_0 = \sqrt{\frac{3}{4}\frac{\dot{M}}{\pi\rho_c v_w^3}} \tag{3}$$

where ρ_c is the core density, v_w is the terminal velocity, and $\dot{M} = 0.5\,\dot{p_w}^2/L_w$ is the mass loss rate from the central cluster. This typically lasts for xx yr.

The initial internal thermal energy of the bubble assuming an adiabatic interior is E_0, the wind velocity v_0,

the shock discontinuity separating free-streaming stellar wind from the hot bubble R_1,

$$v_0 = \frac{L_w}{\dot{p_w}} \tag{4}$$

$$R_0 = v_0 t_0 \tag{5}$$

$$E_0 = \frac{5}{11}L_w t_0 \tag{6}$$

$$T_0 = L_{w,36}^{8/35} n^{2/35} t_6^{-6/35}\,(1-\zeta)^{2/5} \tag{7}$$

where $L_{w,36} = L_w/10^{36}\,{\rm erg\,s^{-1}}$, $t_6 = t_0/10^6\,{\rm yr}$ and $\zeta \equiv r/R_0$ ($r \to R_0$).

The main parameters which we track are the radius, the velocity, the energy, and the temperature.

3.2. Phase I: Energy-driven

The initial phase is characterised with the following energy and momentum equations

At early phase, the bubble radius R_2, the inner and outer shell radius is somewhat entangled. The shell is very thin, and there is not much swept up mass.

The inner shock region R_1 is given by

$$R_1 = \sqrt{\frac{F}{2E}\,(R_2^3 - R_1^3)} \tag{8}$$

The pressure calculation is of great academic interest. Add citation here (ash, deb, mcleod etc).

Here

$$P_{ram} = \frac{3L_{bol}}{4\pi R^2 c} \tag{9}$$

what is different pressure? others are isotropic but gravity not, just because it has the same units. doaginal along the SE tensor.

One important factor is the rate at which mass evaporates from the outer shell into the hot bubble (e.g., see Cowie & McKee 1977)

We keep track of the rate at which mass evaporates from the shell into the hot ionised region

$$\frac{dM_b}{dt} = \lim_{r\to R_2} 4\pi r^2 \frac{\mu p}{k}\frac{\alpha r/t - v}{T} \tag{10}$$

which, as described in Weaver et al. (1977), has to satisfy these sets of equations corresponding to the velocity and temperature structure of the bubble:

$$T = \left(\frac{25}{4}dM_b/dt\frac{k}{4\pi R_2^2\mu C}\right)^{2/5}(R_2 - r)^{2/5} \tag{11}$$

$$\frac{\partial T}{\partial r} = -\frac{2}{5}\frac{T}{R_2 - r} \tag{12}$$

$$v = \frac{\alpha R_2}{t} - dM_b/dt\frac{kT}{4\pi R_2^2 \mu p} \tag{13}$$

At the beginning, cooling is kept constant, as its effect is not large. Alpha, beta, and delta values are constant. After some time, we need to find them via root algorithms. When cooling is important, these values must be calculated and deviate.

The bubble is loses energy at some rate Edot = E/cs, where cs is the sound crossing time.

MacLow-Mccray

The shocked ISM will become thermally unstable and collapse into a thin shell when its radiative cooling time scale becomes less than the age of the system. $t_c = 3nkT/(nnLambda(T))$. This means that a cold shell will form after a very short time (e.g., see Castor et al. 1975; Mac Low & McCray 1988)

Cooling time scale for the interior is approximately the time at which the total energy radiated becomes comparable to the total energy contained in the interior.

evaporation of the swept-up shell into the hot shocked wind region may cause strong radiative cooling and lead to the end of the energy-dominated regime

3.3. Phase II: Momentum-driven

At this point the bubble has lost all energy, and the shell is purely driven by momentum.

Two things can happen: the shell expands into the ISM until it dissolves, or the shell collapses.

We implement fragmentation mechanism in the future.

the pressure term now becomes momentum (ram) instead of energy (E2P), see Sam Geen.

3.4. Phase III: Collapse or dissolution?

The bubble can have two fates: one is that gravity prevails, and the bubble collapses. One is that the bubble expands into the ambient ISM.

We evolve each model until one of two criteria is met. The first is the natural timescale set by the lifetimes of the massive stars responsible for driving the expansion. Until the latest possible stage of supernovae explosions. The

second is spatial: we stop the calculation once the bubble expands to a point where it can no longer be regarded as a coherent structure, and instead merges with the surrounding ISM.

To this end, we adopt a fiducial value of 20 Myr and 500 pc

In future versions of the code we plan to include fragmentation mechanisms, which represent another pathway for the bubble to lose energy and maintain a coherent structure. These include gravitational fragmentation of the swept-up shell, Rayleigh–Taylor instabilities, and the formation of low-density channels that allow feedback energy to leak into the ambient ISM.

Another possibility is to include a sequential star formation. This could either happen at unity, or at shell fragmentation.

4. Heating and cooling mechanisms

photodissociation?

As the bubble expands, cooling takes place. In this section, we shed light on how cooling is being treated in TRINITY.

We treat cooling in a simple two-temperature manner. For temperature $<$ 104K, the gas is said to be in CIE. Therefore only the temperature is required for this.

At temperature 10$>$4, for example due to ionising radiation from stars, gas is often not in CIE.

We use similar cooling curves as described in Rahner et al. (2018)

4.1. Effects on bubble structure

The bubble velocity and temperature profile is modified (Weaver) according to the inclusion of cooling.

$$\alpha = \frac{d\ln R_2}{d\ln t}, \quad \beta = -\frac{d\ln p}{d\ln t}, \quad \delta = \left(\frac{\partial \ln T}{\partial \ln t}\right)_{\xi} \tag{14}$$

The introduction of these variables lead to the following:

$$\frac{1}{pr^2}\frac{\partial}{\partial r}\left(CT^{5/2}r^2\frac{\partial T}{\partial r}\right) - \frac{5}{2}\left(v - \frac{\alpha r}{t}\right)\frac{1}{T}\frac{\partial T}{\partial r} - \frac{n_e n \Lambda}{p} = \frac{\beta + 2.5\delta}{t} \tag{15}$$

$$\frac{1}{r^2}\frac{\partial}{\partial r}\left(r^2 v\right) - \left(v - \frac{\alpha r}{t}\right)\frac{1}{T}\frac{\partial T}{\partial r} = \frac{\beta + \delta}{t} \tag{16}$$

It is then obvious that cooling affects the temperature and kinematics of the bubble and the shell, and the temperature and kinematic profiles in turn affect the cooling.

5. Variations in the initial cloud density profile

To run our simulations, we first specify the initial density profile of the cloud. TRINITY provides two options for this setup. The first is a simple power-law density profile, which offers flexibility and computational simplicity but has limited physical motivation. The second is an isothermal sphere in hydrostatic equilibrium, corresponding to a Bonnor–Ebert configuration, which more closely reflects the observed structure of real molecular clouds. In this section, we describe how each profile is implemented in TRINITY and how their corresponding mass distributions are computed.

5.1. Power-law profile

A simple power-law density distribution is described as follows:

$$\rho_{\rm cl}(r) = \begin{cases} \rho_c & \text{if } r \le r_c, \\ \rho_c \left(\dfrac{r}{r_c}\right)^{\alpha} & \text{if } r_c < r \le r_{\rm cl}, \\ \rho_{\rm ISM} & \text{if } r > r_{\rm cl}. \end{cases}$$

where $r_{\rm cl}$ denotes the cloud radius, r_c is the core radius and $\rho_{\rm amb}$ is the ISM density. We allow values $-2 \le \alpha \le 0$, with a focus on $\alpha = 0, 2$. In the case of $\rho \propto r^0$, we are effectively modelling a homogeneous gas cloud, in which ρ_c denotes its average density. While such a configuration does not necessarily represent a physical molecular cloud, it serves as a useful limiting case to highlight the capability of TRINITY in the simplest possible setting. For the case of $\rho \propto r^{-2}$ we have the classic singular isothermal sphere (e.g., Larson 1969; Shu 1977; Whitworth et al. 1996), where ρ_c denotes the core density, with core radius in the range of $r_c = 0.1 - 0.01$ pc, consistent with observational studies of nearby molecular clouds (e.g., see Könyves et al. 2015; Zhang et al. 2018; Massi et al. 2019; Nony et al. 2023)

The resulting cloud mass enclosed within radius r is simply:

$$M(r_{\rm cl}) = 4\pi \int_0^{r_{\rm cl}} r^2 \rho(r)\, {\rm d}r \tag{17}$$

5.2. Bonnor-Ebert profile

In most cases, a simple power-law density profile does not provide an adequate description of molecular clouds. Observations (e.g., Alves et al. 2001; Johnstone et al. 2000; Burkert & Alves 2009; Haworth et al. 2015) instead indicate that their density structure is well represented by solutions corresponding to pressure-confined, self-gravitating isothermal spheres in hydrostatic equilibrium. These configurations, often referred to as Bonnor–Ebert spheres (Bonnor 1956; Ebert 1955; Hartmann 1998), are critically stable according to the Bonnor–Ebert criterion and provide a better physical basis for modelling molecular gas structures (e.g., see Kirk et al. 2006; Burkert & Alves 2009; Zier et al. 2021).

A Bonnor-Ebert sphere - under spherical symmetry - has to fulfill the following equations of hydrostatic equilibrium, Poisson's equation and the isothermal equation of

state:

$$\frac{dP}{dr} = -\rho(r)\frac{GM(r)}{r^2} \tag{18}$$

$$\frac{1}{r^2}\frac{d}{dr}\left(r^2\frac{d\Phi}{dr}\right) = 4\pi G\rho(r) \tag{19}$$

$$P = \rho c_s^2 \tag{20}$$

Combining these equations (see Appendix) we arrive at a variant of the Lane-Emden equation:

$$\frac{1}{\xi^2}\frac{d}{d\xi}\left(\xi^2\frac{d\psi}{d\xi}\right) = e^{-\psi} \tag{21}$$

where $\xi = \left(\frac{4\pi G\rho_c}{c_s^2}\right)^{1/2} r$ is the non-dimensional radial parameter, ρ_c is the core density, $c_s = \sqrt{k_B T/\mu}$ is the isothermal sound speed and $\psi(\xi) = \Phi/c_s^2$. The equation can then be numerically solved with the following boundary conditions:

$$\psi(0) = 0, \quad \left.\frac{d\psi}{d\xi}\right|_{\xi=0} = 0 \tag{22}$$

giving us the density profile in the form of

$$\rho(r) = \rho_c \exp -\psi(\xi) \tag{23}$$

There exist a value $\xi_{\max}$ such that beyond it a gas cloud would be unstable and prone to gravitational collapse. Thus we set a default value of critical density contrast $\Omega_{\max} = \rho_c/\rho_{\rm cl} = 14.1$ for our simulations, corresponding to a dimensionless radius of $\xi_{\max} = 6.45$, beyond which equilibrium models do not exist and gravitational collapse must ensue[1]. Following 2 we have the Bonnor-Ebert mass:

$$M(\xi_{\max}) = 4\rho_c^{-1/2}\left(\frac{c_s^2}{4\pi G}\right)^{3/2}\left(\xi^2\frac{d\psi}{d\xi}\right)_{\xi=\xi_{\max}} \tag{24}$$

5. Numerical Implementation How the BE sphere is discretized in simulation: Density table interpolation or direct integration of the Lane–Emden equation. How pressure confinement is modeled. Boundary conditions and central resolution.

The BE sphere is initialised in the following manner: Given a density contrast, it calculates the sound speed required such that both Equation (mass) holds.

[1] There is, however, some leeway for departures from strict Bonnor–Ebert stability. In particular, modest oscillations around the critical state are expected, driven by additional physical effects such as internal magnetic pressure or external pressure arising from turbulence, nearby stellar winds, and radiation, which can act as stabilizing mechanisms beyond purely thermal support (e.g., see Alves et al. 2001). These effects broaden the range of conditions under which clouds can persist without undergoing rapid collapse.

5.2.1. Comparison

Given that we have different, it is therefore interesting to see how our selection of density profile affects the outcome of our simulation. A one-to-one comparison does not really make sense, as for a given cloud mass, the density profile directly influences its radius. One way to test this is to set up initial conditions such that the clouds have the same radius. Another is such that the clouds have the same mass.

We have performed three suites of simulations. The first suit explores the consequences of changing... The second we explore, with a view to determining the effect of density ..

In Figure xx we present a comparison between bubbles of similar radius. Even though both shell reaches similar value, we see that the initial conditions are very different, i.e., the cloud density. This shows that even something s simple as initial profile can influence the values.

In Figure xx we show instead two clouds of same initial condition and see how it evolves.

In Figure xx we show initial value of cloud radius, given parameters. These all have sfe of 1% I think.

In conclusion, the selected density profile affects profoundly the outcome of the simulation.

6. Shell structure and dynamics

Massive winds and radiation pressure sweep up interstellar gas into thin expanding shells that traps radiation - this can strongly affect the dynamics and structure of the shell, and the distribution of gas within. Here, we provide the set of equations with which we use to describe how radiation interacts with the swept-up shell (see also Draine 2011; Martínez-González et al. 2014; Rahner et al. 2017):

$$\frac{d}{dr}\left(\frac{\mu_n}{\mu_p}n_{\rm sh}kT_i\right) = \frac{1}{4\pi r^2 c}\frac{d}{dr}\left(L_n e^{-\tau_d} + L_i\phi\right) \tag{25}$$

$$\frac{d\phi}{dr} = -\frac{4\pi r^2}{Q_i}\alpha_B n_{\rm sh}^2 - n_{\rm sh}\sigma_d\phi \tag{26}$$

$$\frac{d\tau_d}{dr} = n_{\rm sh}\sigma_d \tag{27}$$

where $n_{sh}(r)$ is the shell gas density, $T_i = 10^4\,\mathrm{K}$ is the ionised gas temperature, Q_i is the rate of ionising photons emitted by the central cluster, L_i, L_n are the ionising and non-ionising luminosities respectively, where $L_i + L_n = L_{\rm bol}$ is the bolometric luminosity. We set $\sigma_d = 1.5 \times 10^{-21}\,\mathrm{cm}^2$ (Draine 2011) as the dust absorption cross section per hydrogen atom, and assume a case-B recombination with a coefficient $\alpha_B = 2.59 \times 10^{-13}\,\mathrm{cm}^3\mathrm{s}^{-1}$ (Osterbrock & Ferland 2006). We obtain the star cluster feedback parameters (i.e., L_i, L_n, Q_i) directly with STARBURST99 (Leitherer et al. 1999).

Here, Equation (25)[2] describes how gas pressure responds to momentum deposition due to ionising radiation, $L_i\phi$, and the interaction of non-ionising photons on dust grains, $L_n e^{-\tau_d}$. Equation (26) describes radiation-gas coupling, showing how ionising photons decreases as they move outward through the shell. Ionizing photons are removed

[2] In contrast to the H II region treatment of Draine (2011), we drop the $\alpha_B n^2\langle h\nu\rangle/c$ contribution: the momentum carried by recombination photons is negligible compared to direct radiation and dust absorption in driving the expansion of both ionised and neutral shell layers.

both by recombinations and by dust absorption at a rate proportional to $\alpha_B n_{sh}^2$ and $n_{sh}\sigma_d\phi$ respectively. Finally, Equation (27) shows the optical depth along the line of sight.

The term σ_d describes how effective dust grains attenuate in the radiation field, and we set as a constant value, where in reality this value may differ in different environments. Lower-metallicity galaxies will have lower values, simply because there is less material out of which to form grains. It is also a function of stellar temperature and decreases when stars die. For simplicity, we take the effective cross section as a scaling of metalicity $\sigma_{eff} = Z/Z_\odot\sigma_d$.

We set the boundary conditions for the equations as follows: we assume the central cluster has evacuated a low-density cavity, so absorption inside this zone is negligible. Such idealisation is common in modelling H II regions (e.g., see Kewley & Dopita 2002; Draine 2011; Martínez-González et al. 2014). Thus, we impose the conditions $\phi(0) = 1$ and $\tau(0) = 0$, and integrate outward until the ionizing budget is exhausted (i.e., $\phi(r) \to 0$).

Once the shell grows sufficiently thick, the ionisation front slows down; the outer layer therefore cools and form a neutral layer that is dynamically coupled to the radiation field predominantly through dust absorption of the non-ionising continuum that leaks from the interior. In this regime, the equations above simplify to:

$$\frac{d}{dr}\left(n_{\rm sh}kT_a\right) = \frac{1}{4\pi r^2 c}\frac{d}{dr}\left(L_n e^{-\tau_d}\right) \tag{28}$$

$$\frac{d\tau_d}{dr} = n_{\rm sh}\sigma_d \tag{29}$$

where the composition within the neutral shell is $\mu_n/\mu_p \simeq 1$. Hence, in this limit, the neutral shell's acceleration is governed predominantly by the coupling between dust and non-ionising flux - ionizing photons play no further dynamical role beyond maintaining the thin inner ionized layer.

Finally, we note that the ion number density at the inner edge of the ionised shell is P_s thermal pressure at inner radius of shell:

$$n_s(t) = \frac{\mu_a P_s}{\mu_i kT_i} \tag{30}$$

As mentioned in Section 3.3, the evaporation of shell into the shocked wind region may cause strong radiative cooling. This leads to the end of energy-dominating phase, and we have a transition into momentum-driven phase. This gives us:

$$n_s(t) = \frac{\mu_a P_{ram}}{\mu_i kT_i} \tag{31}$$

7. ISM Pressure

For most cases, the impact of the ISM pressure has negligible effect on shell dynamics - until the shell reaches beyond the edge of the molecular cloud. Once the velocity of the shell expansion becomes comparable with the sound speed in the ambient ISM,

$c_s \sim \surd$

The effect becomes significant when the shell expansion velocity approaches sht sound speed of the ambient ISM.

We also do not consider the impact that the ambient pressure has on the shell dynamics, as it is only significant when the shell expansion ve- locity approaches the sound speed value in the ambient ISM. The distribution of the ionized gas then becomes quasi-static and is defined by the values of thermal pressure at the inner edge of the shell and in the ambient ISM, as was discussed in the previous section. In the supersonic regime, which is the case in all our calculations (see Mach number values in the captions to Figures 3 and 4, calculated under the assumption that the sound speeds in the ionized and neutral ISM are 15 km s1 and 1.04 km s1 , respectively), the rate of mass accumula- tion by the expanding shell depends on the speed of the leading shock, Vs (Pedge/ISM) 1/2 , where Pedge is the thermal pressure value immediately behind the leading shock and ISM is the gas density in the ambient ISM. The impact of the external pressure on the shell dynamics is thus negligible in this case.

The impact of ISM pressure is non-trivial on the evolution of bubble radius. We include a parameter for users to input.

Simulations - 1. 0 ISM pressure. Shell expands infinitely and explodes - 2. 5e3 something. Shell expansion is halt/smaller.

$$P_{\rm amb} = \begin{cases} P_0 + \dfrac{\mu_i}{\mu_p} n_{\rm cl}(R_2) kT_i & \text{if } f_{{\rm esc},i} > 0, \\ P_0 & \text{otherwise.} \end{cases} \tag{32}$$

Does external pressure explain recent results for molecular clouds? (Field et al. 2011) ranges of 10e4 - 10e7

To imitate different surroundings, we can also have the sphere in higher turbulence (see Debs paper?).

This setup mimics a range of star-forming environments by varying the ambient ISM pressure, demonstrating that in turbulent, high-pressure conditions, the feedback-driven bubble can undergo recollapse. Such recollapse events may lead to the formation of a subsequent generation of stars, highlighting the potential role of environment-dependent feedback regulation in clustered star formation.

8. Plots

8.1. Impact of ISM pressure on homogeneous radius

8.2. Initial cloud radius for different density profiles

8.3. Density profile (in similarly collapsing cloud)?

8.4. visualising TRINITY phases

9. Discussion

- Physics not covered: mag field, turbulence, cosmic rays.
- Preliminary website: TRINITY
- Future: IMF stochasticity. Metallicity.

References

Alves, J. F., Lada, C. J., & Lada, E. A. 2001, Nature, 409, 159
Bonnor, W. B. 1956, MNRAS, 116, 351
Burkert, A. & Alves, J. 2009, ApJ, 695, 1308
Castor, J., McCray, R., & Weaver, R. 1975, ApJ, 200, L107
Cowie, L. L. & McKee, C. F. 1977, ApJ, 211, 135
Draine, B. T. 2011, ApJ, 732, 100
Ebert, R. 1955, ZAp, 37, 217
Field, G. B., Blackman, E. G., & Keto, E. R. 2011, MNRAS, 416, 710
Hartmann, L. 1998, Accretion Processes in Star Formation, Vol. 32
Haworth, T. J., Facchini, S., & Clarke, C. J. 2015, MNRAS, 446, 1098

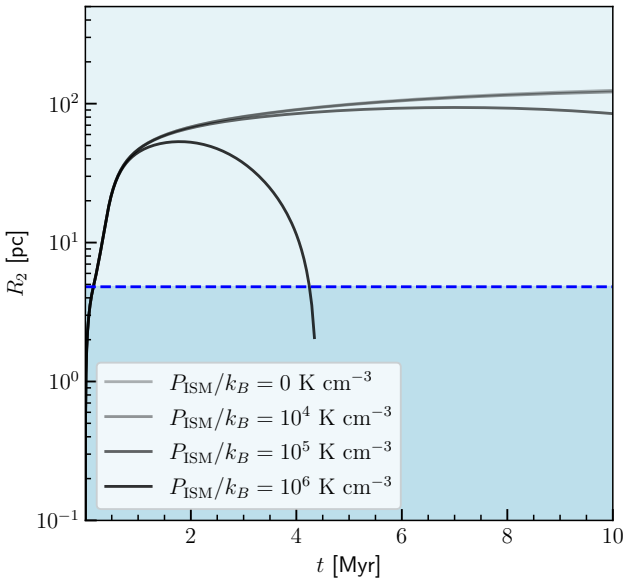

Fig. 1. Evolution of feedback-driven bubble radius beyond molecular cloud ($r_{cl} = 3.76$ pc) under varying ISM pressure conditions. As external pressure increases, the expansion of the bubble slows; beyond a critical pressure threshold, the bubble's growth stalls and reverses, leading to collapse.

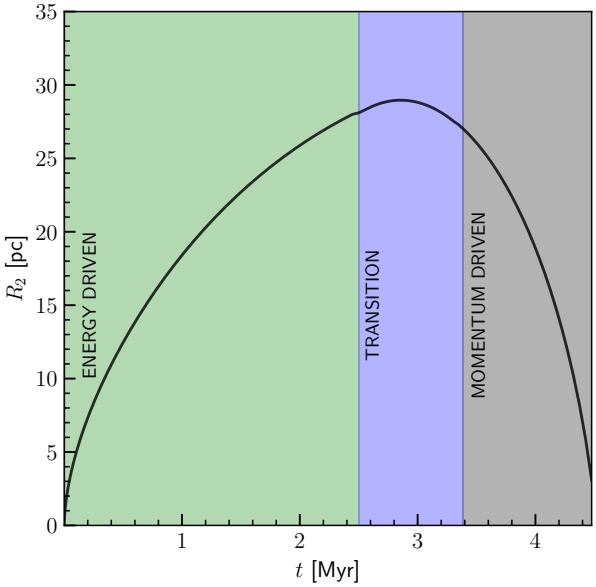

Fig. 3. Visualisation of three different TRINITY phases across bubble evolution. Run: xx sol mass, xx density, xx sphere profile. cloud radius = xx. In this particular scenario, the collapse of bubble happens right after cooling is comparable to input luminosity.

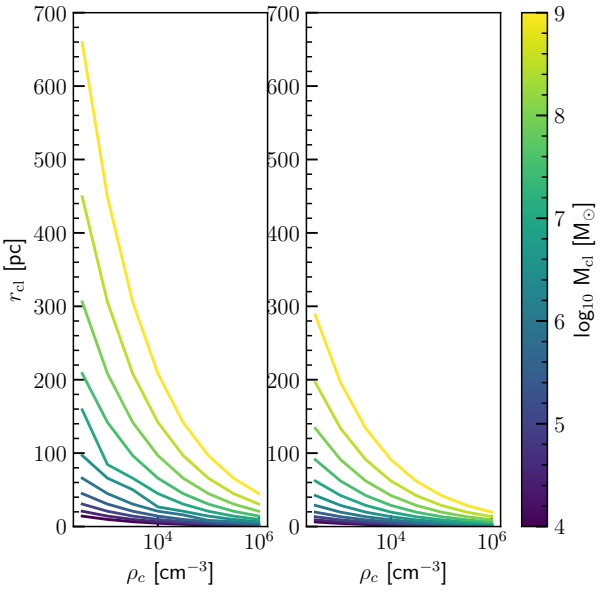

Fig. 2. Comparison of Bonnor-Ebert profile vs. homogeneous cloud profile. For a given cloud mass and cloud core density, the radius of BE spheres are higher than homogeneous spheres.

Johnstone, D., Wilson, C. D., Moriarty-Schieven, G., et al. 2000, ApJ, 545, 327
Kewley, L. J. & Dopita, M. A. 2002, ApJS, 142, 35
Kirk, H., Johnstone, D., & Di Francesco, J. 2006, ApJ, 646, 1009
Könyves, V., André, P., Men'shchikov, A., et al. 2015, A&A, 584, A91
Lamers, H. J. G. L. M. & Cassinelli, J. P. 1999, Introduction to Stellar Winds
Larson, R. B. 1969, MNRAS, 145, 271
Lee, J. C., Whitmore, B. C., Thilker, D. A., et al. 2022, ApJS, 258, 10
Leitherer, C., Schaerer, D., Goldader, J. D., et al. 1999, ApJS, 123, 3
Mac Low, M.-M. & McCray, R. 1988, ApJ, 324, 776
Martínez-González, S., Silich, S., & Tenorio-Tagle, G. 2014, ApJ, 785, 164
Massi, F., Weiss, A., Elia, D., et al. 2019, A&A, 628, A110
Nony, T., Galván-Madrid, R., Motte, F., et al. 2023, A&A, 674, A75
Osterbrock, D. E. & Ferland, G. J. 2006, Astrophysics of gaseous nebulae and active galactic nuclei
Pathak, D., Leroy, A. K., Thompson, T. A., et al. 2025, ApJ, 982, 140
Rahner, D., Pellegrini, E. W., Glover, S. C. O., & Klessen, R. S. 2017, MNRAS, 470, 4453
Rahner, D., Pellegrini, E. W., Glover, S. C. O., & Klessen, R. S. 2018, MNRAS, 473, L11
Shu, F. H. 1977, ApJ, 214, 488
Watkins, E. J., Kreckel, K., Groves, B., et al. 2023, A&A, 676, A67
Weaver, R., McCray, R., Castor, J., Shapiro, P., & Moore, R. 1977, ApJ, 218, 377
Whitworth, A. P., Bhattal, A. S., Francis, N., & Watkins, S. J. 1996, MNRAS, 283, 1061
Zhang, G.-Y., Xu, J.-L., Vasyunin, A. I., et al. 2018, A&A, 620, A163
Zier, O., Burkert, A., & Alig, C. 2021, ApJ, 915, 7

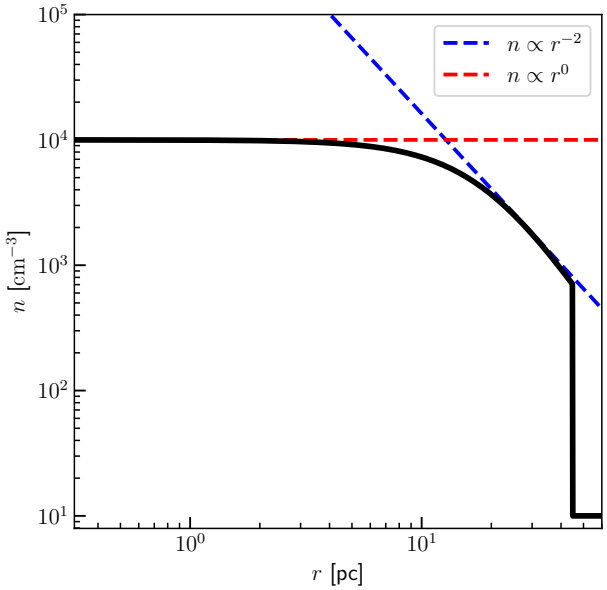

Fig. A.1. Density profile. Density begins with homogeneous to a power-law like profile at high radius. Abrupt cutoff due to cloud radius as additional criteria.

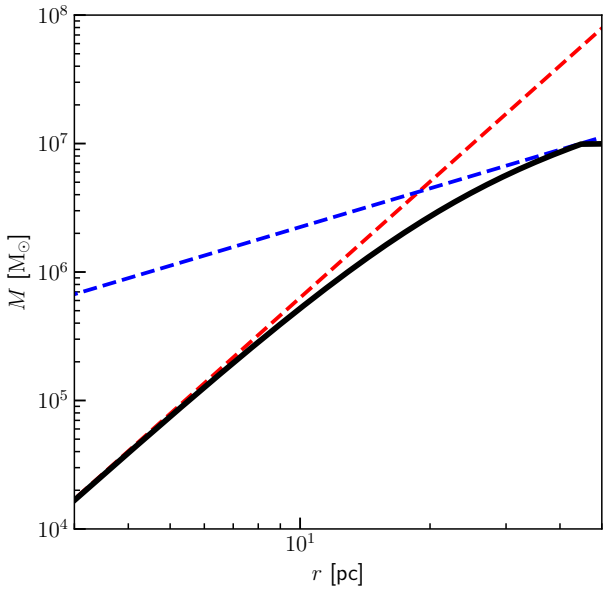

Fig. A.2. Mass profile.

Appendix A: BE visualisation

We provide a visualisation here. As we can see, the sphere tends towards a characteristic r-2.